A&A 570, A31 (2014)
DOI: 10.1051/0004-6361/201323155

Astronomy & Astrophysics

The extended ROSAT-ESO Flux Limited X-ray Galaxy Cluster Survey (REFLEX II)

IV. X-ray luminosity function and first constraints on cosmological parameters⋆

Hans Böhringer[1], Gayoung Chon[1], and Chris A. Collins[2]

[1] Max-Planck-Institut für extraterrestrische Physik, 85748 Garching, Germany
e-mail: hxb@mpe.mpg.de
[2] Astrophysics Research Institute, Liverpool John Moores University, IC2, Liverpool Science Park, 146 Brownlow Hill, Liverpool L3 5RF, UK

Received 29 November 2013 / Accepted 3 April 2014

ABSTRACT

The X-ray luminosity function that is closely related to the cluster mass function is an important statistic of the census of galaxy clusters in our Universe. It is also an important means to probe the cosmological model of our Universe. Based on our recently completed REFLEX II cluster sample comprising 910 galaxy clusters with redshifts we construct the X-ray luminosity function of galaxy clusters for the nearby Universe and discuss its implications. We derived the X-ray luminosity function of the REFLEX II clusters on the basis of a precisely constructed selection function for the full sample and for several redshift slices from $z = 0$ to $z = 0.4$. In this redshift interval we find no significant signature of redshift evolution of the luminosity function. We provide the results of fits of a parameterized Schechter function and extensions of it which provide a reasonable characterization of the data. We also use a model for structure formation and galaxy cluster evolution to compare the observed X-ray luminosity function with the theoretical predictions for different cosmological models. The most interesting constraints can be derived for the cosmological parameters Ω_m and σ_8. We explore the influence of several model assumptions on which our analysis is based. We find that the scaling relation of X-ray luminosity and mass introduces the largest systematic uncertainty. From the statistical uncertainty alone we can constrain the matter density parameter, $\Omega_m \sim 0.27 \pm 0.03$ and the amplitude parameter of the matter density fluctuations, $\sigma_8 \sim 0.80 \pm 0.03$. Marginalizing over the most important uncertainties, the normalisation and slope of the $L_X - M$ scaling relation, we have larger error bars and a result of $\Omega_m \sim 0.29 \pm 0.04$ and $\sigma_8 \sim 0.77 \pm 0.07$ (1σ confidence limits). We compare our results with those of the SZ-cluster survey provided by the *Planck* mission and we find very good agreement with the results using *Planck* clusters as cosmological probes, but there is some tension with *Planck* cosmological results from the microwave background anisotropies, which we discuss in the paper. We also make a comparison with results from the SDSS cluster survey, several cosmological X-ray cluster surveys, and recent Sunyaev-Zel'dovich effect surveys. We find good agreement with these previous results and show that the REFLEX II survey provides a significant reduction in the uncertainties compared to earlier measurements.

Key words. galaxies: clusters: general – cosmological parameters – X-rays: galaxies: clusters

1. Introduction

As the largest, clearly defined objects in our Universe, galaxy clusters are interesting astrophysical laboratories and important cosmological probes (e.g. Sarazin 1986; Borgani et al. 2001; Voit 2005; Vikhlinin et al. 2009; Allen et al. 2011; Böhringer 2011). They are particularly good tracers of the large-scale structure of the cosmic matter distribution and its growth with time. While most of the precise knowledge on the galaxy cluster population has come from X-ray observations as explained in the above references, recent progress has also been made by optical cluster surveys (e.g. Rozo et al. 2010) and millimetre wave surveys using the Sunyaev-Zel'dovich effect (Reichardt et al. 2012; Benson et al. 2013; Marriage et al. 2011; Sehgal et al. 2011; Planck Collaboration VIII 2011; Planck Collaboration XVI 2014). X-ray surveys for galaxy clusters are still the most advanced by providing statistically well defined, approximately mass-selected cluster samples, since: (i) X-ray luminosity is tightly correlated to mass (e.g. Reiprich & Böhringer 2002; Pratt et al. 2009); (ii) bright X-ray emission is only observed for evolved clusters with deep gravitational potentials; (iii) the X-ray emission is highly peaked and projection effects are minimized; and (iv) for all these reasons the survey selection function can be accurately modelled.

The ROSAT All-Sky Survey (RASS, Trümper 1993) is the only existing full-sky survey conducted with an imaging X-ray telescope, providing a sky atlas in which one can systematically search for clusters in the nearby Universe. The largest high quality sample of X-ray-selected galaxy clusters has been provided so far by the REFLEX Cluster Survey (Böhringer et al. 2001, 2004, 2013) based on the southern extragalatic sky of RASS at declination ≤2.5 degree. The quality of the sample has been demonstrated by showing that it can provide reliable measures of the large-scale structure (Collins et al. 2000; Schuecker et al. 2001; Kerscher et al. 2001), yielding cosmological parameters (Schuecker et al. 2003, 2003; Böhringer 2011) in good agreement within the measurement uncertainties with

⋆ Based on observations at the European Southern Observatory La Silla, Chile.

the subsequently published WMAP results (Spergel et al. 2003; Komatsu et al. 2011). The REFLEX data have also been used to study the X-ray luminosity function (XLF) of galaxy clusters (Böhringer et al. 2002), the galaxy velocity dispersion – X-ray luminosity relation (Ortiz-Gil et al. 2004), and the statistics of Minkowski functionals in the cluster distribution (Kerscher et al. 2001) and to select statistically well defined subsamples like the HIFLUGCS (Reiprich & Böhringer 2002) and REXCESS (Böhringer et al. 2007). The latter is particularly important as a representative sample of X-ray surveys to establish X-ray scaling relations (Croston et al. 2008; Pratt et al. 2009, 2010; Arnaud et al. 2010) and the statistics of the morphological distribution of galaxy clusters in X-rays (Böhringer et al. 2010).

Recently we have completed an extension of REFLEX except for 11 missing redshifts, REFLEX II, which roughly doubles the size of the cluster sample. The construction of this sample is described in Böhringer et al. (2013). In the present paper we describe the construction of the REFLEX II XLF from the galaxy cluster data and the survey selection function derived in Böhringer et al. (2013). We fit parameterized functions to the data and we compare the observed luminosity function to the predictions of cosmological structure formation models. From the latter comparison we obtain constraints on cosmological parameters. The most sensitive of these parameters are the matter density parameter, Ω_m, and the amplitude parameter of the matter density fluctuations, σ_8. We focus on deriving robust constraints on the two parameters in this paper, while leaving a comprehensive modelling of the combined uncertainty of all relevant cosmological and cluster parameters to a future publication. We study the errors introduced by various other uncertainties instead case by case and evaluate the overall systematic errors. The REFLEX II cluster sample has also been used recently to construct the first supercluster catalogue for clusters with a well defined selection function (Chon & Böhringer 2013), showing among other results that the XLF of clusters in superclusters is top-heavy in comparison to that of clusters in the field.

A preliminary sample of REFLEX II that had 49 fewer redshifts than used here, has been applied to the study of the galaxy cluster power spectrum by Balaguera-Antolinez et al. (2011). The results show very good agreement with the cosmological predictions based on cosmological parameters determined from WMAP 5 yr data. In a second paper (Balaguera-Antolinez et al. 2012), in which the construction of REFLEX mock samples from simulations used in the earlier paper is described, a preliminary XLF of REFLEX II has been determined. Here we use a completely new approach with updates on the cluster sample, the scaling relations, and the missing flux correction used in the sample construction, with the survey selection function based on the procedures described in Böhringer et al. (2013).

Other previous determinations of the XLF of galaxy clusters include: Piccinotti et al. (1982); Kowalski et al. (1984); Gioia et al. (1984, 2001); Edge et al. (1990); Henry et al. (1992); Burns et al. (1996); Ebeling et al. (1997); Collins et al. (1997); Burke et al. (1997); Rosati et al. (1998); Vikhlinin et al. (1998); De Grandi et al. (1999); Ledlow et al. (1999); Nichol et al. (1999); Donahue et al. (2001) Allen et al. (2003); Mullis et al. (2004); Böhringer et al. (2007); Koens et al. (2013).

The paper is organized as follows. In Sect. 2 we introduce the REFLEX II galaxy cluster sample and the survey selection function. In Sect. 3 we use the parameterized Schechter function fitted to our data to describe the resulting XLF. In Sect. 4 we outline the cosmological modeling used for the theoretical prediction of the cluster mass and XLF. In Sect. 5 we discuss the results of the model comparison to the data for different cosmological models. The effect of the uncertainties in the used cluster scaling relations on the results is discussed in Sect. 6 and other systematic uncertainties of our analysis are discussed in Sect 7. In Sect. 8 we compare our results to findings from other surveys and Sect. 9 closes the paper with the summary and conclusions.

If not stated otherwise, we use a geometrically flat Λ-cosmological model with $\Omega_m = 0.3$ and $h_{70} = H_0/70\ \mathrm{km\,s^{-1}\,Mpc^{-1}} = 0.7$ for the calculation of physical parameters and survey volumes. All uncertainties without further specifications refer to 1σ confidence limits.

2. The REFLEX II galaxy cluster survey

The REFLEX II galaxy cluster survey is based on the detection of galaxy clusters in the RASS (Voges et al. 1999). The region of the survey is the southern sky below equatorial latitude +2.5 deg at galactic latitude $b_{II} \geq 20$ deg. The regions of the Magellanic clouds have been masked. The survey region selection, the source detection, the galaxy cluster sample definition and compilation, and the construction of the survey selection function as well as tests of the completeness of the survey are described in Böhringer et al. (2013). In brief the survey area is ~2.4 ster or 13 924 square degrees. The nominal flux limit down to which galaxy clusters have been identified in the RASS in this region is 1.8×10^{-12} erg s^{-1} cm^{-2} in the 0.1−2.4 keV energy band. For constructing the XLF in this paper we impose an additional cut on the minimum number of detected source photons of 20 counts. This has the effect that the nominal flux cut quoted above is only reached in about 80% of the survey and in regions with lower exposure and higher interstellar absorption the flux limit is accordingly higher (see Fig. 11 in Böhringer et al. 2013). This effect is modelled and considered in the survey selection function.

The flux limit imposed on the survey is for a nominal flux, which has been calculated from the detected photon count rate for a cluster X-ray spectrum characterized by a temperature of 5 keV, a metallicity of 0.3 solar, a redshift of zero, and an interstellar absorption column density given by the 21 cm sky survey described by Dickey & Lockmann (1990). This count rate to flux conversion is appropriate prior to any redshift information and is analogous to an observed object magnitude corrected for galactic extinction in the optical.

After the redshifts have been measured, a new flux is calculated taking the redshifted spectrum and an estimate for the spectral temperature into account. The temperature estimate is obtained from the X-ray luminosity – temperature relation of Pratt et al. (2009) determined from the REXCESS cluster sample, which is a sample of clusters drawn from REFLEX I for deeper follow-up observations with *XMM-Newton* and which is representative of the entire flux-limited survey (Böhringer et al. 2007). The luminosity is determined first from the observed flux by means of the luminosity distance for a given redshift. Using the X-ray luminosity mass relation given in Pratt et al. (2009) we can then use the mass estimate to determine a fiducial radius of the cluster, which is taken to be r_{500}[1]. We then use a beta model for the cluster surface brightness distribution to correct for the possibly missing flux in the region between the detection aperture of the source photons and the radius r_{500}. The procedure for determining the flux, the luminosity, the temperature estimate, and r_{500} is done iteratively and described in detail

[1] r_{500} is the radius where the average mass density inside reaches a value of 500 times the critical density of the Universe at the epoch of observation.

in Böhringer et al. (2013). In that paper we deduced a mean flux uncertainty for the REFLEX II clusters of 20.6%, which is mostly due to the Poisson statistics of the source counts, but it also contains some systematic errors. For the following analysis, we adopt a flux and luminosity measurement uncertainty of 20%.

The X-ray source detection and selection is based on the official RASS source catalogue by Voges et al. (1999). We have been using the publicly available final source catalogue[2] as well as a preliminary source list that was created while producing the public catalogue. The latter source list had a lower significance limit and included a larger number of detections, but it had not been manually screened as the public data set. This ensured a higher completeness of the input catalogue and spurious sources were caught by our subsequent screening. Since the analysis software used to produce the public RASS source catalogue is tuned for point sources and does not perform very well for the extended sources of galaxy clusters, we analyzed all the X-ray sources again with the growth curve analysis method (Böhringer et al. 2000). The flux cut was imposed on the reanalysed data set. The results of the flux determination was inspected visually for all sources above, and near the flux limit and for pathological cases, as well as cases of source confusion, the results were corrected manually.

The galaxy clusters among the sources have been identified using all available means: X-ray source properties, available optical images (mostly from DSS[3]), literature data (mostly from NED[4]), and finally follow-up observations at ESO La Silla. The source identification scheme is described in detail in Böhringer et al. (2013). The redshifts were secured mostly by multi-object spectroscopy and the redshift accuracy of the clusters is typically 60 km s^{-1} (Guzzo et al. 2009; Chon & Böhringer 2012).

The survey selection function is a very important survey product that is crucial for this paper. We constructed the selection function in the form of a survey mask that provides the limiting X-ray luminosity for the cluster detection as a function of the sky position and redshift. For the sky position the survey mask is currently given in pixels of one square degree. The survey mask takes all the systematics of the RASS exposure distribution, galactic absorption, the fiducial flux, the detection count limit, and all the applied corrections described above into account. The survey mask is given in three-dimensional form so that it can also be used for any study that is related to the spatial distribution of the clusters. A preliminary version of it has been used for the construction of the cluster density distribution power spectrum and a preliminary construction of the luminosity function in Balaguera-Antolinez et al. (2011, 2012). It furthermore allows a cluster sample to be selected from simulations in a precisely analogous way to the REFLEX II survey selects the clusters from the sky.

The survey selection function provides the means to calculate the effective survey volume as a function of the X-ray luminosity. This survey volume function is shown in Fig. 1 for different imposed redshift limits. The objects with the lowest X-ray luminosities are only detected in a small volume in the nearby Universe due to the flux limit of the survey. The luminous clusters with $L_X \geq 2.5 \times 10^{44}$ erg s^{-1} are found in a volume larger than 1 Gpc^3. We also show the survey volume

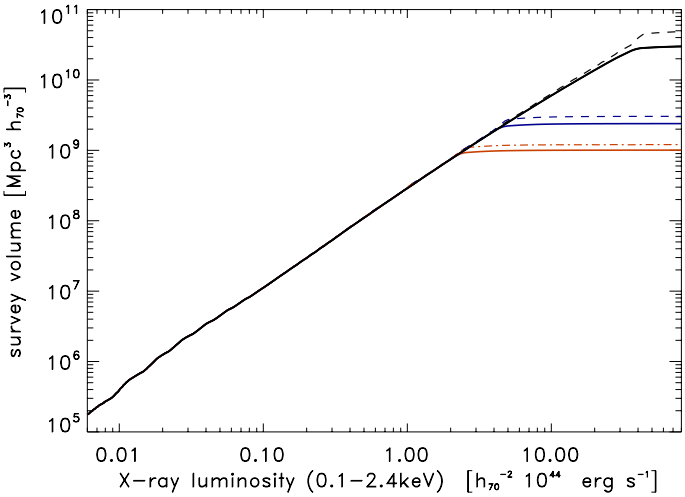

Fig. 1. Effective survey volume as a function of X-ray luminosity. The survey volume was calculated for three different cut-off redshifts, $z = 0.8$, $z = 0.3$, $z = 0.22$ for our reference cosmology ($h = 0.7$, $\Omega_m = 0.3$ and $\Omega_\Lambda = 0.7$). We also determined the same set of curves for a cosmology with the parameters $h = 0.7$, $\Omega_m = 0.26$ and $\Omega_\Lambda = 0.74$ shown as dashed curves. The difference between the set of curves has been amplified by a factor of 10, to make the offset more visible. This affects the dashed curves that are shown slightly offset from the original position.

calculated for two different cosmological models in the figure including the reference cosmology used in the paper ($h = 0.7$, $\Omega_m = 0.3$ and $\Omega_\Lambda = 0.7$) and a cosmology closer to the WMAP results (Komatsu et al. 2011) with parameter values of $h = 0.7$, $\Omega_m = 0.26$ and $\Omega_\Lambda = 0.74$. The difference is rather small and we have exaggerated the difference between the curves representing the two cosmologies by a factor of 10 to make it more visible. The largest difference is found for the survey volume at the cut-off redshift, since at lower redshifts the effect of the cosmological model on the deduced luminosity and survey volume partly compensate producing very similar curves.

In the following we use different versions of these calculations, to also determine the selection function in redshift shells. For the proper cosmological modelling of the results, we determine the survey volume for any given cosmology used in the model fitting process.

3. The X-ray luminosity function

The XLF is determined from the catalogue of clusters and the survey selection function in the form of the effective survey volume as a function of X-ray luminosity as shown in Fig. 1. We use a source detection count cut of minimum 20 photons for the selection. Then the binned differential XLF is given by

$$\frac{\mathrm{d}n(L_X)}{\mathrm{d}L_X} = \frac{1}{\Delta L_X} \sum_i \frac{1}{V_{max}(L_{X_i})} \quad (1)$$

where V_{max} is the effective detection volume and ΔL_X is the width of the luminosity bin and the sum includes all clusters in the bin. Figures 2 and 3 show the XLF derived for a binning with 20 clusters per bin, except for the bin at the lowest X-ray luminosity, for different redshift ranges, while Fig. 2 presents the XLF in four equidistant redshift shells from $z = 0$ to $z = 0.4$.

The luminosity values used in the construction of the XLF are the luminosities inside r_{500}, corrected for missing flux in the 0.1−2.4 keV rest frame band. The errors for the XLF given in the

[2] The RASS source catalogs can be found at: http://www.xray.mpe.mpg.de/rosat/survey/rass-bsc/ for the bright sources and http://www.xray.mpe.mpg.de/rosat/survey/rass-fsc/ for the faint sources

[3] See http://archive.stsci.edu/dss/

[4] See http://ned.ipac.caltech.edu/

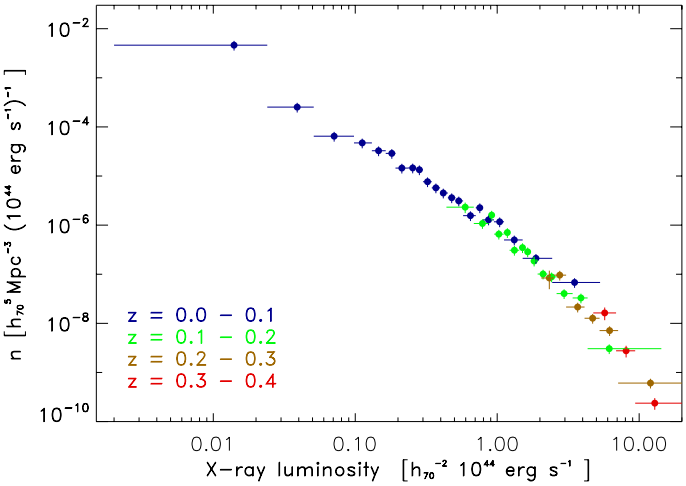

Fig. 2. X-ray luminosity function of REFLEX II determined in four equidistant redshift shells from $z = 0$ to $z = 0.4$. Owing to the flux limit of the sample, the different redshift shells cover different luminosity ranges. In the overlap region the functions show no major differences.

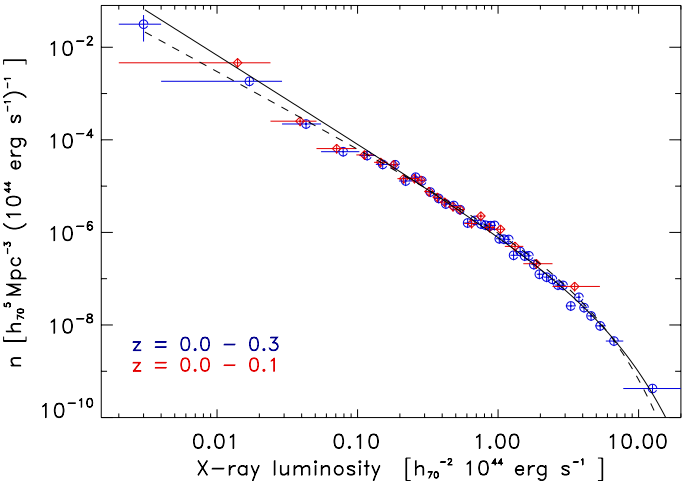

Fig. 3. X-ray luminosity function of the REFLEX II galaxy cluster survey averaged over the survey volumes out to redshifts $z = 0.1$ and $z = 0.3$. Schechter functions have been fitted to the two data sets separately to visualize the potential difference of the functions. The fits were performed over the full observed X-ray luminosity range.

figures are the Poisson uncertainties for the number of clusters per bin.

When looking for evolutionary effects in the XLF in Fig. 2, we do not detect any significant difference in the functions, which implies no severe deficiencies in the cluster detection in the high redshift shells and no strong evolutionary effects. What is expected from theory is mostly a change at the high luminosity end, where the lower redshift shells should show more luminous clusters than the more distant ones. In Appendix A we show the expectation for our best fitting cosmological model. While the mass function would show a more noticeable change with redshift, the corresponding change in the XLF is small since the evolution effect is partly compensated for by the adopted redshift evolution of the X-ray luminosity – mass relation. In the theoretical functions we see a significant difference only at luminosities above about $6 \times 10^{44}\ h_{70}^{-2}$ erg s^{-1} where we have hardly any objects and no statistics in the two lowest redshift shells below $z = 0.2$.

Figure 3 compares the XLF in the two redshift ranges from $z = 0$ to $z_{\rm max} = 0.1$ and $z_{\rm max} = 0.3$. There are 419 clusters at $z < 0.1$ and 802 clusters at $z < 0.3$ for $L_{\rm X} \geq 3 \times 10^{42}$ erg s^{-1}. In the larger volume at $z > 0.3$ there are 53 additional clusters. Constructing the XLF in an even larger volume (e.g. for $z_{\rm max} = 0.8$) shows hardly any difference in the resulting function. To make it even clearer that there is not much leverage to look for redshift evolution in the data, we fit Schechter functions to the two data sets (as will be explained in the next section), which are also shown in the figure. The Schechter fit prefers a slightly less top-heavy luminosity function for the lowest redshift bin. We therefore do not pursue a detailed modelling of the evolution of the XLF any further in this paper and assume that the XLF can be described reasonably well by a constant function in the redshift range $z = 0$–0.4.

3.1. Fits of a Schechter function

For an analytical, phenomenological description of the REFLEX XLF we fit a Schechter function of the form

$$n(L_{\rm X})\,{\rm d}L_{\rm X} = n_0 \left(\frac{L_{\rm X}}{L_{\rm X}^*}\right)^{-\alpha} \exp\left(-\frac{L_{\rm X}}{L_{\rm X}^*}\right) \frac{{\rm d}L_{\rm X}}{L_{\rm X}^*} \tag{2}$$

to the data.

We use a maximum likelihood method to determine the best fitting Schechter function parameters by comparing the predicted and observed X-ray luminosity distribution of the galaxy clusters. The approach we take is similar to what we used in Schuecker & Böhringer (1998); and Böhringer et al. (2002; see also Daley & Vere-Jones 1988; and for a similar application Marshall et al. 1983; and Henry 2004). To test a distribution function, $\lambda(x)$, with discrete observational data points, $\lambda(x_i)$, we minimize the likelihood function:

$$\ln L = -\int \lambda(x){\rm d}x + \sum_{i=1}^{N} \ln \lambda(x_i). \tag{3}$$

The distribution function $\lambda(x)$ should describe observables. In our case we compare the observed and predicted X-ray luminosity distribution of the clusters. The X-ray luminosities can be considered to be almost direct observables, because the spectral model assumptions used for their derivation are safe and possible changes have very little influence on the resulting luminosities. Before the comparison, the predicted X-ray luminosity distribution, $N(L_{\rm X})$, is folded with the observational error in the following way:

$$N(L_{\rm X}) = \int_{L_{\rm Xmin}}^{\infty} n(L'_{\rm X}) V_{\rm max}(L'_{\rm X}) \Psi(L'_{\rm X}, L_{\rm X})\,{\rm d}L'_{\rm X} \tag{4}$$

where $n(L'_{\rm X})$ is the Schechter luminosity function and $\Psi(L'_{\rm X}, L_{\rm X})$ represents the Gaussian error distribution for the mean measurement uncertainty of 20%.

Figure 4 shows the luminosity distribution function and the fit for the redshift range $z \leq 0.3$ and the luminosity range $L_{\rm X} \geq 10^{43}$ erg s^{-1}. The uncertainties of the fit for the two most important parameters, α and $L_{\rm X}^*$ are shown in Fig. 5, where we give the 1 and 2σ constraints. The typical 1σ uncertainties – similar for fits in different X-ray luminosity ranges – are $\Delta\alpha = 5\%$ and $\Delta L_{\rm X}^* = 22\%$.

The XLF is now observationally so well constrained, that a Schechter fit is no longer an adequate description. Studying the fits for varying X-ray luminosity ranges as shown in Table 1, we

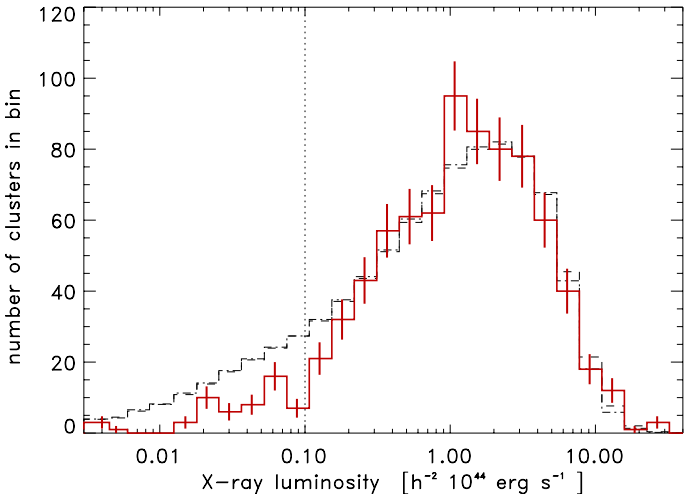

Fig. 4. X-ray luminosity histogram of the REFLEX II clusters at $z \leq 0.3$ (red line with error bars) compared to the best fitting Schechter function for the X-ray luminosity range $L_X \geq 0.1 \times 10^{44}$ erg s^{-1}. The X-ray luminosity limit is indicated by the vertical dotted line. The error bars give the Poisson uncertainty of the counts in the bins.

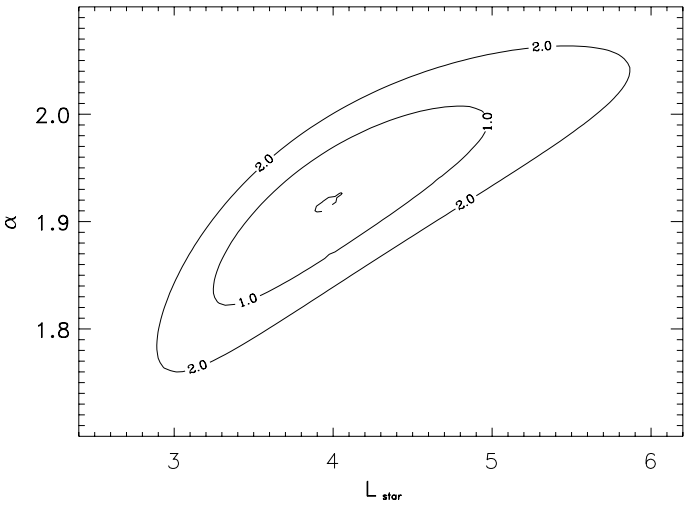

Fig. 5. Constraints on the Schechter parameters α and L_X^* from the fit to the data of the X-ray luminosity function of REFLEX II for $z \leq 0.3$ and luminosity range $L_X \geq 0.1 \times 10^{44}$ erg s^{-1}.

note that fits limited to the higher luminosity side of the luminosity function require a steeper slope, and the fit is forced to a shallower slope for the full range of X-ray luminosities, at the expense of a worse fit in the high and intermediate luminosity ranges.

3.2. Alternative fitting functions

Since the Schechter function does not provide such a satisfying analytical description of the REFLEX II XLF, we have also tried alternative functions for the fit. As already used in our previous paper by Balaguera-Antolinez (2012) we apply a q-exponential function of the following form:

$$n(L_X)\mathrm{d}L_X = n_0 \left(\frac{L_X}{L_X^*}\right)^{-\alpha} \left[1 + \frac{L_X}{L_X^*}(1-q)\right]^{\frac{1}{1-q}} \frac{\mathrm{d}L_X}{L_X^*}. \quad (5)$$

The effect of the q-exponential function is to cause a sharper decrease of the Schechter function at high luminosities. This extra degree of freedom helps to improve the fit as can be seen in Table 1.

Table 1. Best fitting parameters for a Schechter function and alternative functions to the REFLEX II X-ray luminosity function.

Method	L_x–range	α	L_X^*	n_0	q	η	No. cl.
A	≥0.003	1.74	3.02	5.0×10^{-7}	–	2.3	802
A	≥0.01	1.76	3.10	4.7×10^{-7}	–	2.5	798
A	≥0.03	1.78	3.19	4.5×10^{-7}	–	2.9	779
A	≥0.1	1.93	3.99	2.8×10^{-7}	–	9.9	741
A	≥0.3	2.03	4.67	2.0×10^{-7}	–	24.3	623
B	≥0.003	1.54	1.08	1.8×10^{-6}	1.39	1.4	802
B	≥0.01	1.53	1.03	2.0×10^{-6}	1.39	1.4	802
B	≥0.1	1.60	1.17	1.6×10^{-6}	1.39	2.5	802
C	≥0.003	2.19	5.7	1.3×10^{-7}	–	1.6	802
C	≥0.01	2.18	5.5	1.4×10^{-7}	–	1.6	798
C	≥0.03	2.13	5.0	1.7×10^{-7}	–	1.4	779
C	≥0.1	2.18	5.4	1.4×10^{-7}	–	1.7	741
C	≥0.3	2.17	5.4	1.4×10^{-7}	–	1.6	623

Notes. The method code *A* is for the Schechter function (Eq. (2)), *B* for the q-exponential (Eq. (5)) and *C* for the modified Schechter function (Eq. (6)). The X-ray luminosity range used in the fit and the parameter L_X^* are given in units of 10^{44} h_{70}^{-2} erg s^{-2}. α, L_X^*, and n_0 (in units of h_{70}^3 Mpc^{-3}) are the slope, the break parameter, and the normalization of the Schechter function or its modified variants, while q is the extra parameter of the q-exponential function. η is similar to a reduced χ^2 parameter determined as explained in the text and the last column gives the number of clusters involved in the fit. The typical uncertainties are ~5% for α and ~22% for L_x.

To estimate how well the fit reproduces the data we calculate the squared difference of the observed number of clusters in luminosity bins compared to the one predicted using Eqs. (2), (5), and (6) nomalized by the Poisson error of the observations. We derive a parameter denoted η that is the sum of the squared normalized differences over all bins, divided by the number of bins. This is very similar to a reduced χ^2, with the difference that we do not normalize by the degrees of freedom. We prefer to use the parameter η since we want to characterize the deviation from the data rather than the statistical significance of the fit. The summation is carried out only over those bins with either a detection of at least one cluster or a predicted number larger than 0.1. The values are given in Table 1. While the fit is performed using data in the given luminosity range, the η parameter is always given for the full luminosity range. One clearly notes the improvement in the fit for the q-exponential function. Comparing the fit for the q-exponential function with the earlier fitting results of Balaguera-Antolinez (2011), which are converted to our cosmology model as $\alpha = 1.54$, $L_X^* = 1.2 \times 10^{44}$ h_{70}^{-2} erg s^{-1}, $n_0 = 1.4 \times 10^{-6}$ h_{70}^3 Mpc^{-3}, and $q = 1.3$, we find good agreement given that the sample was completed with additional cluster redshifts and that the scaling relations used were slightly improved.

Probably an even better way to arrive at a stable fit is to decrease the slope of the fitting function towards low luminosities. For this reason we also tried another modification of the Schechter function that bends the function down at very low luminosities. This modified function has the form:

$$n(L_X)\mathrm{d}L_X = n_0 \left(\frac{L_X}{L_X^*}\right)^{-\alpha} \exp\left(-\frac{L_X}{L_X^*}\right) \left[1 - \left(1 + \frac{L_x}{\beta}\right)^{-\gamma}\right] \frac{\mathrm{d}L_X}{L_X^*} \quad (6)$$

where $\beta = 0.25$ and $\gamma = 1.7$ are extra parameters. Rather than determining these two extra parameters in an overall fit, we found

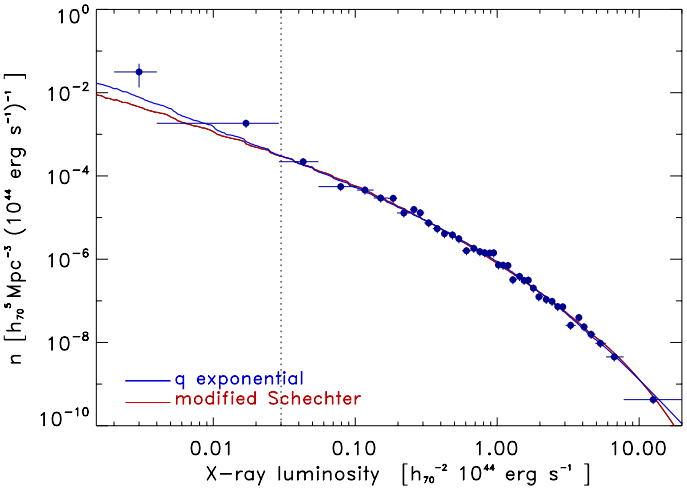

Fig. 6. X-ray luminosity function of REFLEX II for a redshift limit of $z = 0.3$ fitted by a q-exponential function and by the modified Schechter function. Both fits were performed for the X-ray luminosity range $L_X \geq 0.03 \times 10^{44}$ erg s^{-1} indicated by the vertical dotted line.

suitable parameters before the final fit. This keeps the number of fit parameters small, avoids degeneracies, and thus allows for a better comparison of the different fitting results.

We note that the fits are stabler and we basically recover a good fitting function for the whole luminosity range even if the fit is restricted to $L_X \geq 0.3 \times 10^{44}$ erg s^{-1}. Therefore we consider the fitting results of this function as our best description, at least for the luminosity range $L_X \geq 0.02 \times 10^{44}$ erg s^{-1}. The fits for the q-exponential and the modified Schechter function are shown in Fig. 6. The fits do not describe the first two data points that lie outside the fitted range very well, but these bins only contain 23 clusters all together and we put most emphasis on a good fit for the rest of the data.

3.3. Comparison to previous determinations of the X-ray luminosity function

Previously determined XLF at low redshift generally show good agreement with the REFLEX I XLF within the error limits of these smaller cluster samples. This includes in particular the low redshift part of the RDCS, 400 deg^2, and WARPS surveys (Rosati et al. 2002; Mullis et al. 2004; Koens et al. 2013, and further references therein). The REFLEX I survey is in good agreement with the present results. The Schechter function fit presented for REFLEX I in Böhringer et al. (2002) is close to the present fit in the luminosity range $L_X \geq 3 \times 10^{42}$ erg s^{-1}. The small difference is that the REFLEX I function is slightly lower at low values of L_X, which is due to a better sampling of the poor groups in REFLEX II, and REFLEX I slightly overshoots at high values of L_X, which is mostly due to a small decrease in the scaling radius for massive clusters with the new scaling relations. These small changes do not affect the agreement with previous results for the XLF.

4. Model predictions of the cluster X-ray luminosity function

The XLF of galaxy clusters can be used to obtain constraints on cosmological model parameters, notably on the matter density parameter Ω_m and the amplitude parameter of the dark matter density fluctuations, σ_8. For determining these parameters we need to compare the prediction of the XLF for specific cosmological models with our observations. In this section we describe our method for this prediction.

Table 2. Default cosmological model parameters.

Parameter	Explanation	Value
h_{100}	Hubble parameter	0.7
Ω_b	baryon density	0.045
n_s	Primodial $P(k)$ slope	0.96
α_{sl}	$L_X - M$ relation slope	1.51
n_0	$L_X - M$ relation norm.	0.1175
mass bias	X-ray mass underestimation	0.1

Notes. In addition to the parameters we assume the model describes a flat ΛCDM Universe.

In the first step of the calculations we determine the cluster mass function based on the recipe given by Tinker et al. (2008). A prerequisite for this calculation is to specify the statistics of the large-scale structure in the form of the dark matter density fluctuation power spectrum. For the shape of the power spectrum we assume that the initial power spectrum in the early Universe is described by a power law with slope of 0.96, which is consistent with the latest result from the *Planck* mission (Planck Collaboration XVI 2014). We model the structure evolution to the present epoch by a transfer function as given by Eisenstein & Hu (1998) including baryonic acoustic oscillations for a baryon density of $\Omega_b = 0.045$. The amplitude of the power spectrum is specified by the amplitude parameter, σ_8. This parameter is the variance of the fluctuation field filtered with a top-hat filter, as shown in Eq. (7) below, with a radius of 8 h^{-1} Mpc. For the formula of the mass function we calculate the variance of the filtered field through

$$\sigma^2(R_F) = \frac{1}{2\pi^2} \int P(k) \tilde{W}^2_{TH}(R_F, k) k^2 \mathrm{d}k \qquad (7)$$

where $P(k)$ is the power spectrum at the epoch of consideration, $\tilde{W}_{TH}(R_F, k)$ is the top hat filter in Fourier space with filter radius R_F in real space, and $\sigma(R_F)^2$ is the variance of the density fluctuation field. The variance as a function of filter radius can be transformed into a function of mass using the mean density of the Universe, $\bar{\rho}_m$. The filter mass is given by $M = \frac{4\pi}{3} \bar{\rho}_m R_F^3$, and the mass function can then be written by

$$\frac{\mathrm{d}n}{\mathrm{d}M} = f\left[\sigma(M)\right] \frac{\bar{\rho}_m}{M} \frac{\mathrm{d}\ln \sigma^{-1}}{\mathrm{d}M} \qquad (8)$$

with

$$f\left[\sigma(M)\right] = A \left[\left(\frac{\sigma}{b} \right)^{-a} + 1 \right] \exp\left(\frac{c}{\sigma^2} \right). \qquad (9)$$

Here M is the mass of the dark matter haloes or clusters in terms of an overdensity of 180 over the mean density of the Universe, $\bar{\rho}_m$. We use for the overdensity the value of 180 and the following values for the open parameters in Eq. (9), $A = 0.186$, $a = 1.47$, $b = 2.57$, and $c = 1.19$ as given in Table 2 of Tinker et al. (2008). Some of these parameters are assumed to have a redshift dependence. We use the following parametrizations, $A(z) = A_0(1+z)^{-0.14}$, $a(z) = a_0(1+z)^{-0.06}$, and $b(z) = b_0(1+z)^{-\alpha}$ with $\log \alpha = \left[\frac{0.75}{\log(\Delta/75)} \right]^{1.2}$.

The mass given by this equation is the mass inside a mean overdensity of 180 above the mean density of the Universe. We

use masses defined for a mean overdensity of 200 above the critical density of the Universe at the epoch of light emission of the observed object. Therefore we have to transform the mass equation into our definition. For the conversion we assume that the mass profile of all clusters can be described by an NFW-model profile (Navarro et al. 1995, 1997) with a concentration parameter of five.

We use the following conventions throughout the paper. We will use an overdensity of 200 over the critical density of the Universe to characterize the mass of the clusters (which is actually an intermediate parameter that is not essential for the final results), because this mass is closer to what we usually understand as the virial mass. The X-ray parameters, like the X-ray luminosity, are given inside a radius of r_{500}, because this is closer to the observed aperture in which X-ray luminosity is observationally determined. We do not introduce an inconsistency by using different fiducial radii for mass and luminosity as long as we have a careful book-keeping of all the convertions and scaling relations.

We then use an empirical mass – X-ray luminosity scaling relation of the form

$$L_{500}(0.1\text{–}2.4\ \mathrm{keV}) = 0.1175\ M_{200}^{\alpha_{\rm sl}}\ h^{\alpha_{\rm sl}-2}\quad E(z)^{\alpha_{\rm sl}} \qquad (10)$$

where $\alpha_{\rm sl}$ is the slope of the scaling relation, and $E(z) = H(z)/H_0$ is the evolution parameter related to the Hubble constant. The unit for L_{500} is $10^{44}\ h_{70}^{-2}$ erg s^{-1} (0.1–2.4 keV), and for M_{200} it is $10^{14}\ h_{70}^{-1}\ M_\odot$. The redshift evolution of this relation is based on the assumption of no evolution of the $L_{\rm X} - T$ relation. For a discussion of this choice, see Böhringer et al. (2012). We also take into account that this relation has an intrinsic scatter with a preferred value of $\log \sigma_{L_{\rm X}} = 0.114$, which corresponds to about 30%. We go on to fold in an observational error of the luminosity of 20% which is the fractional mean error in the flux determination of the REFLEX II cluster sample (Böhringer et al. 2013).

For the slope of the $L_{\rm X} - M$ scaling relation, $\alpha_{\rm sl}$, we explore two values, 1.51 and 1.61 to illustrate our uncertain knowledge. The value of 1.61 is motivated by the results of our REXCESS study (Pratt et al. 2009) and the analysis of Vikhlinin et al. (2009). For REXCESS a lower value of 1.53 is obtained before the assumed Malmquist bias correction. In comparison to several other studies these values for the slope are on the high side (see our survey of the topic in Böhringer et al. 2012). For example the complete HIFLUGCS sample of 63 clusters gives a value of 1.46 and the extended HIFLUGCS a value of 1.61 (Reiprich & Böhringer 2002). Maughan (2007) finds 1.45 in their cosmological analysis. Mantz et al. (2008) find a best fitting value of 1.24. We therefore prefer the value 1.51 as the best compromise for all the data and for the relatively large and homogeneous HIFLUGCS sample as our prime value.

For the work in this paper we calculated the predicted luminosity function for the median redshift of the REFLEX II cluster sample of $z = 0.102$ and quote the corresponding cosmological parameters for $z = 0$. For modelling these two different epochs, we used the standard formulae for the linear growth of the density fluctuation field, since it is the linear fluctuation evolution that is accounted for in the applied statistical theory.

With these ingredients we can predict the XLF analytically for different cosmological models. For any variation in the cosmological model away from our reference model, we had to convert the input X-ray luminosities, the values of $V_{\rm max}$ with the corresponding survey selection function, and the scaling relations to the new cosmology.

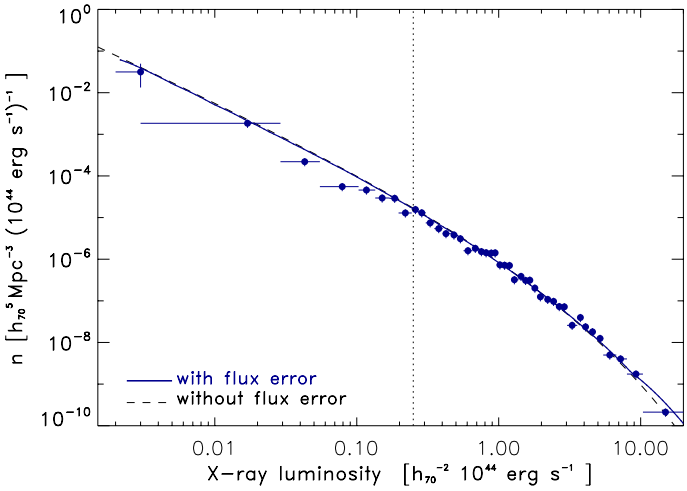

Fig. 7. X-ray luminosity function of REFLEX II (data points) and the predicted X-ray luminosity function for the best fitting cosmological model.

5. Cosmological parameters from the REFLEX X-ray luminosity function

To determine the cosmological model parameters that fit our observations best, we use a likelihood function method in an analogous way to the one used for the fitting of the Schechter function in Sect. 3.1. We are again comparing the predicted and observed distribution function of X-ray luminosities, since this is very close to an observable, because the spectral model assumptions used for their derivation introduce only negligible new uncertainties except for changes in the assumed geometry of the universe, which are taken into account. Thus we derive the following predicted distribution function, and it also accounts for the scatter in the $L_{\rm X} - M$ scaling relation

$$\lambda(L_{\rm x}) = \int n(L''_{\rm X})\ V_{\rm surv}(L''_{\rm X})\ \Phi(L''_{\rm X}, L'_{\rm X})\ \ \Psi(L'_{\rm X}, L_{\rm X})\ {\rm d}L''_{\rm X}{\rm d}L'_{\rm X} \qquad (11)$$

where $n(L_{\rm X}) = \frac{{\rm d}n(L_{\rm X})}{{\rm d}L_{\rm X}}$ is the differential XLF and $V_{\rm surv}$ the volume in which clusters with luminosity $L_{\rm X}$ can be found. In case of no redshift constraints the latter is equal to $V_{\rm max}$, while $\Phi(L''_{\rm X}, L'_{\rm X})$ is the scatter in the $L_{\rm x} - M$ relation and $\Psi(L'_{\rm X}, L_{\rm X})$ is the uncertainty of the flux or luminosity measurement.

Figure 7 shows the observed XLF compared to the best fitting model prediction, where only clusters with $L_{\rm x} \geq 0.25 \times 10^{44}\ h_{70}^{-2}$ erg s^{-1} and $z \leq 0.4$ have been used in the fit. This involves 698 clusters in total including the lower total count limit of 20 source photons. Over the fitted range the two functions show very good agreement. The reason for using a restricted luminosity range for this fit is, that for lower values of $L_{\rm X}$, which corresponds to the regime of galaxy groups, we have no reliable constraints on the $L_{\rm X} - M$ relation. It is too dangerous to rely on the assumption that the relation is a straight power law over the full range of observed X-ray luminosities.

In this section we are primarily interested in studying the constraints on those cosmological parameters, for which we can get the most interesting information, that is $\Omega_{\rm m}$ and σ_8. We therefore keep other parameters fixed, but we use a Hubble constant of $h = 0.7$, a baryon fraction compared to the critical density of 0.045, and a spectral index of the primordial matter density fluctuation power spectrum of 0.96. In addition we assume the Universe to be flat, described by a ΛCDM model, that is a Dark Energy universe with an equation-of-state parameter

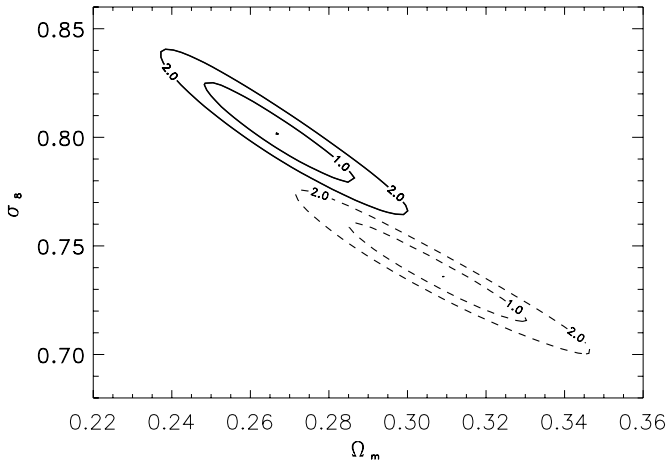

Fig. 8. Constraints of the cosmological model parameters Ω_m and σ_8 from the comparison of the observed REFLEX II X-ray luminosity distribution and the cosmological model predictions. Two results are shown for an $L_X - M$ relation slope of 1.51 (upper ellipses) and 1.61 (lower dashed ellipses). The contour lines show 1σ and 2σ confidence limits.

Table 3. Fit parameters of the best fitting cosmological model prediction to the REFLEX II X-ray luminosity function.

Fit	$L_X - M$ slope	Ω_m	σ_8
$L_X \geq 0.25$	1.51	$0.27 \pm 10\%$	$0.80 \pm 3.5\%$
$L_X \geq 0.25$	1.61	0.31 ± 10	$0.73 \pm 3.5\%$
$L_X \geq 0.25$	marginalized	$0.29 \pm 14\%$	$0.77 \pm 9\%$

Notes. The first column shows the luminosity range used in the fit, while the redshift range is $z \leq 0.4$. The second column gives the slope of the $L_X - M$ relation used in the fit for the model prediction of the XLF. For the results in the third line we have marginalized over the slope and normalization of the scaling relation.

$w = -1$. These values are chosen to be consistent with the nine-year WMAP results and with the *Planck* results (Hinshaw et al. 2013; Planck Collaboration XVI 2014), except for the Hubble constant, which is reported to be 67.8 ± 0.77 for the combined results in the *Planck* publication. We also use a mass bias factor of 0.9 that accounts for the effect that the X-ray determined mass, which is the base of the $L_x - M$ relation in Eq. (10), may be biased low compared to the true mass by about 10%. This has been found in simulations (Nagai et al. 2007; Valdarnini & Piffaretti 2010; Meneghetti et al. 2010) and in comparison to weak lensing results (Mahdavi et al. 2013; Zhang et al. 2010; Okabe et al. 2010). The assumed parameters are summarized in Table 2. We explore the effect of some of these assumptions in a subsequent section.

With these model assumptions, the best constraints for the parameters Ω_m and σ_8 are shown in Fig. 8. We show two results for the significance limits, one for the preferred slope of the $L_x - M$ scaling relation of 1.51 and a second set of contours for a slope value of 1.61. Table 3 summarizes the fitting results. The uncertainties quoted here are only the statistical uncertainties for the constraints on these two parameters alone. There is some degeneracy of the two parameters indicated by the elongated error ellipses, but thanks to the well described shape of the XLF both parameters can be well constrained. Figure B.1 in the Appendix provides an explanation for the behavour of the constraints of Ω_m and σ_8. An increase in Ω_m increases the amplitude of the XLF over the entire luminosity range, and this can

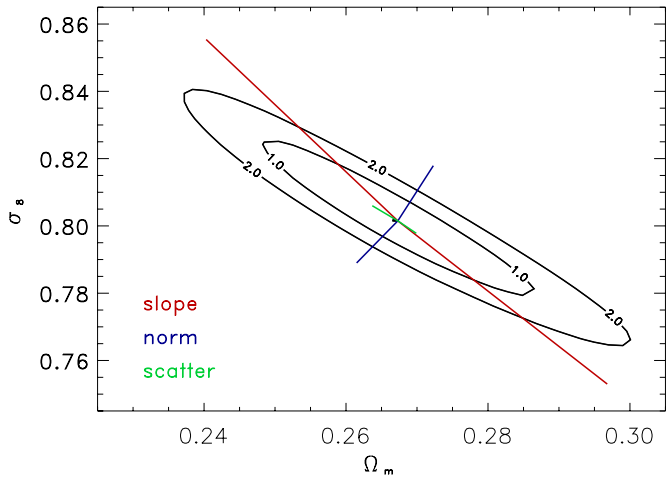

Fig. 9. Variation in the best fitting parameters for Ω_m and σ_8 with a change in slope, scatter, and normalization of the $L_X - M$ scaling relation. The end- and mid-points of the bars give the results for the following values: slope =1.435, 1.51, 1.586 (±5%, largest bars), normalization =0.1292, 0.1175, 0.1058 (±10%, bars in direction of minor axis), scatter =27%, 30%, 33% (±10%, smallest bars).

be partly compensated for by lowering σ_8, but this mostly affects the high luminosity part. This partial compensation leads to the elongated error ellipses, but also allows the degeneracy to be broken.

The lower panel of Fig. B.1 shows the changes in the predicted XLF with the change in the slope of the $L_x - M$ relation. A steeper slope of the relation results in a shallower slope of the XLF. From this behaviour we can predict the change in the best fitting cosmological parameters. A steeper slope of the $L_x - M$ relation can be counteracted by lowering σ_8 with an additional higher value of Ω_m to adjust the normilazation. This is what we observe in Fig. 8.

6. The role of scaling relations

In the last section we have already discussed the influence of the slope of the scaling relation on the cosmological fitting results. A closer inspection of the effect of varying the different model parameters for the fits to the observational data clearly shows that the uncertainties in the scaling relation of observables and mass are the most severe bottle-neck in deriving cosmological constraints from our cluster survey. In Fig. 9 and Table 4 we show the effect of the different parameters characterizing the $L_X - M$ scaling relation used in our modelling. The parameters are the normalization, the slope, and the scatter in the relation. A change in the slope has clearly the strongest effect. It moves the result in a direction very close to the major axis of the error ellipse. A change in the normalization has a less dramatic consequence, but it moves the result in an almost perpendicular direction, more along the minor axis of the error ellipse. Also the scatter has a non-negligible effect on the results. We list the changes in the best fitting model parameters as an effect of changes in the scaling relations in Table 4 in terms of fractional changes and logarithmic derivatives. Since the effect of the uncertainty in the measured flux is the same as that of the scatter of the scaling relations (see Eq. (11)), we also give the result for the fractional change of the combination of the two parameters (assuming that Gaussian error addition applies).

To include these uncertainties for the slope and amplitude of the scaling relation as the most critical parameters in our cosmological constraints, we perform a fit marginalizing over both

Table 4. Dependence of the best fitting values for the cosmological parameters Ω_m and σ_8 on the choice of other model parameters.

Parameter	$\frac{d\ln\Omega_m}{d\ln P}$	$\frac{d\ln\sigma_8}{d\ln P}$	ΔP	$\Delta\Omega_m$	$\Delta\sigma_8$
α_{sl}	2.2	−1.3	10%	22%	13%
n_0	−0.22	−0.18	10%	−2.2%	−1.8%
scatter	0.12	−0.05	10%	1.2%	−0.5%
scatter + ferr.	0.16	−0.07	10%	1.6%	−0.7%
H_0	−0.7	0.4	5%	−3.5%	2%
Ω_b	0.15	−0.07	10%	1.5%	−0.7%
n_s	−0.9	0.5	5%	−4.5%	2.5%
$\Omega_m + \Omega_\Lambda$	$\leq\pm0.11^a$)	≤0.07	5%	≤±0.5%	≤0.35%
f_{mass}	−0.3	−0.28	10%	−3%	−3%
w	≤0.02	≥−0.02	10%	0.15%	−0.19%

Notes. First parameter set: slope α_{sl}, normalization, n_0, and scatter of the $L_X - M$ relation, and scatter combined with the flux error. Second parameter set: H_0, Hubble constant, Ω_b baryon density, n_s slope of the primordial power spectrum, $\Omega_m + \Omega_\Lambda - 1$, degree of the deviation from a flat universe, f_{mass} mass bias, and w, equation-of-state parameter for Dark Energy assumed to be constant. P heading the columns indicates the parameter of the row. $\Delta\Omega_m$ and $\Delta\sigma_8$ give the change in the resulting values for these two parameters upon a parameter variation, ΔP. [(a)] Ω_m decreases with a change of curvature in both directions.

parameters. We allow approximate 1σ uncertainties of 7% for the slope and 14% for the normalization. The uncertainty in the mass bias is equivalent to a corresponding uncertainty in the normalization. Thus this error includes both the amplitude error of the relation of ∼10% and a 10% mass bias uncertainty. The uncertainty of ±7% for the slope of the scaling relation is motivated by the difference in the most reliable results in the literature: the statistically complete HIFLUGCS sample with $\alpha_{sl} = 1.46$, the Pratt et al. (2009) BCES (Y|X) fit with $\alpha_{sl} = 1.53$, and the Vikhlinin et al. (2009) with $\alpha_{sl} = 1.61$. These studies use galaxy cluster samples constructed to be representative of the relevant survey population. We thus take the mean difference of these results as the sigma for the slope variation. We also note that the statistical uncertainties of the slopes quoted in these works has similar magnitude to this difference.

Figure 10 shows the new constraints with relaxed assumptions for the two most critical parameters. The contours enclose a larger area than those of Fig. 8. The 2σ contour is now embedding both error ellipses shown in Fig. 8. One behaviour is noteworthy. The fit of the X-ray luminosity distribution favours a slightly higher value for the slope than 1.51 for the best match of the observed and predicted X-ray luminosity distribution. This shifts the centre of the uncertainty ellipses slightly towards the lower right-hand corner of the plot, the direction of the result for a larger slope. The numerical values of the results are given in Table 3.

7. Other systematic uncertainties

As already mentioned, it is not the aim of this paper to provide a comprehensive marginalization over all uncertainties involved in our analysis since we would like to defer this task to a following publication that uses a more appropriate approach. We prefer to make the effect of the isolated variation of the important parameters transparent. Therefore we studied the dependence of the results for Ω_m and σ_8 on the variation in other cosmological parameters. The results are summarized in Table 4. A parameter with a strong effect is the Hubble constant, H_0. For constant Ω_m a change in the Hubble constant changes the mean density of

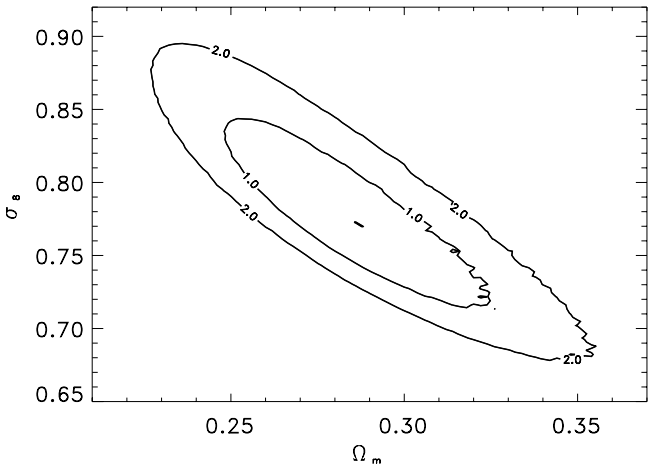

Fig. 10. Constraints of the cosmological model parameters Ω_m and σ_8 for the REFLEX II cluster sample with a marginalization over the most influential model parameters involving the slope, α_{sl}, and the normalization, n_0, of the $L_X - M$ relation. Shown are the 1 and 2σ confidence limits.

the Universe and thus also changes the filter scale (in Eq. (7)) for a cluster of given mass. This explains only part of the effect of H_0, as we found that a change in H_0 cannot be compensated for by a corresponding change in Ω_m. The effect of H_0 is more complex. While the baryon density in the Universe, a possible curvature, and the equation of state parameter w have a very minor influence, the slope of the primordial power spectrum, n_s, is also an important parameter to consider. Finally, the role of f_{mass} has already been discussed, since its effect is the same as that of changing the $L_X - M$ normalization, as can be seen from Eq. (10).

We also checked the effect of sample incompleteness on the results of the cosmological constraints by arbitrarily excluding a fraction of the observed clusters from the sample analysed. The effect of a reduction of the sample by 10% for example decreases Ω_m by 3.5%, and σ_8 increases by less than 0.2%. Thus it is clear that at this stage the sample completeness, which is very high for REFLEX II, is of no concern for the results discussed here.

An inspection of Table 4 again shows that the most dramatic effect on the results comes from the uncertainty of the slope of the $L_X - M$ scaling relation, while the effect of the normalization is amongst the next most important parameters, along with H_0 and n_s. Therefore we are confident that the marginalization over these two most important parameters gives a fair and conservative account of the overall uncertainty of our cosmological constraints.

The relatively weaker effect of these other cosmological parameters on the Ω_m and σ_8 parameters compared to the uncertainties of the scaling relation was also discussed in Voevodkin & Vikhlinin (2004); Vikhlinin et al. (2009); Henry et al. (2009) and Rozo et al. (2010) with the same conclusion.

8. Discussion and comparison to previous results

A comparison of the results on the cosmological parameter constraints shown in Figs. 8 and 10 clearly shows how much information is lost because of our imprecise knowledge of the observable – mass scaling relations. Therefore one of our major efforts in the future will be invested to improve this situation.

One effect not included in the error bars of the XLF given here is the sample variance. This effect is caused by structure on very large scales such that our survey results would be slightly different had data been sampled in exactly the same way in a

different region of our Universe. We estimated the cosmic variance in the same way as in our previous paper on the XLF of REFLEX I (Böhringer et al. 2002) by approximating the survey volume by a sphere. We then calculated the variance of the dark matter density from the power spectrum filtered by a top hat filter with the size of this sphere. This approach and its effects are also described by Hu & Kravtsov (2003). To further estimate the variance effect on the cluster density we also have to account for the fact that the cluster density is biased with respect to the dark matter. This bias factor depends on the X-ray luminosity or the mass of the clusters. The calculations of the bias are based on the formulas by Tinker et al. (2010) and have been described in Balaguera-Antolinez et al. (2011). We find that the sample variance dominates the uncertainties in the cluster density in the XLF at $L_X < 8 \times 10^{42}\ h_{70}^{-2}$ erg s^{-1}. It is less than half at $L_X \sim 2.5 \times 10^{43}\ h_{70}^{-2}$ erg s^{-1}, the lowest luminosity included in our fits, and it decreases rapidly thereafter. Thus we have not corrected for this effect in the present work.

With our conservative approach to marginalization over the most important systematic uncertainties, we can now compare our results to other cosmological studies using galaxy clusters. The findings that are most similar to ours in the way cosmological parameters are constraint are the recently published result obtained with galaxy clusters detected in the *Planck* microwave background survey through the Sunyeav-Zel'dovich effect (SZE, Planck Collaboration XX 2014). This survey is also an all-sky survey. There are 189 galaxy clusters detected at the high signal-to-noise ratio used for the cosmological analysis. Ninty-two percent of the clusters have redshifts $z \leq 0.4$, and 81% have $z \leq 0.3$ compared to our REFLEX II sample where 99% have $z \leq 0.4$ and 92% $z \leq 0.3$. Thus even though the REFLEX II sample on average has lower redshifts, the redshift range is still quite similar. The cosmological analysis for the *Planck* clusters uses a different approach than the one used here. While we have reproduced the luminosity distribution, in the *Planck* analysis the redshift distribution is used to determine the best fit. In the absence of strong evolutionary effects in the galaxy cluster population for the narrow redshift range, the approaches actually do have some similarity. In the probed redshift range in the nearby Universe, the *Planck* cluster sample is approximately flux limited, since the measured integrated SZE is proportional to the apparent surface area of the objects, which is decreasing with the inverse square of the distance for low redshifts. A redshift histogram at low redshift thus reflects the cumulative luminosity function probed at different luminosity cuts. In this sense the two approaches are quite comparable.

There is another similarity between the two surveys. The mass-observable relation for the SZE detected *Planck* clusters relies heavily on the calibration of the X-ray properties of the clusters (see Arnaud et al. 2010; Melin et al. 2011; Planck Collaboration XX 2014). Therefore we actually expect to see constraint results that give a very similar parameter range. Since systematic effects are more important at this current state, the larger size of the REFLEX II sample does not play a major role. Therefore it is, on one hand, not very surprising to see such good agreement between the cosmological constraints from the two surveys as shown in Fig. 11. On the other hand, the cluster detection and selection is very different, and the agreement gives much support to the different survey methods.

In Fig. 11 we also compare the cluster results for the constraints on Ω_m and σ_8 to those derived from the analysis of the microwave background anisotropies as measured with WMAP 9 yr data (Hinshaw et al. 2013) and by the *Planck* mission (Planck Collaboration XVI 2014). As discussed in detail in the

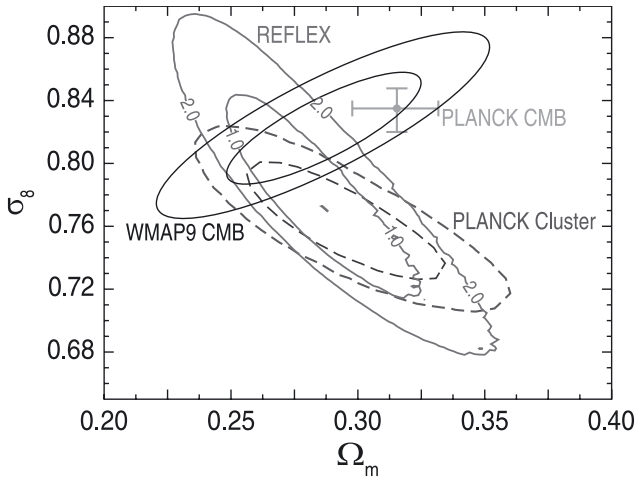

Fig. 11. Comparison of the marginalized cosmological model constraints for the REFLEX II survey with the results from the *Planck* mission for galaxy clusters (Planck Collaboration XX 2014) as well as with the CMB power spectrum (Planck Collaboration XVI 2014) and with the CMB results from the 9 year WMAP data (Hinshaw et al. 2013). The contour lines give the 1σ and 2σ results for the cluster surveys and WMAP mission and the cross gives the 1σ result from *Planck* CMB (Planck Collaboration XVI 2014).

Planck result paper on cosmological constraints from galaxy clusters (Planck Collaboration XX 2014), the two results from *Planck* show some discrepancy. Here we confirm the *Planck* cluster results from X-ray observations, using a somewhat different approach based on the luminosity distribution instead of the redshift distribution of the clusters. In Fig. 11 we show the best cosmological fit for *Planck* CMB data with WMAP polarization data quoted in the *Planck* cosmology paper (Planck Collaboration XVI 2014) with 1σ error bars. This result is closer to the cluster constraints than the error ellipses shown in Planck Collaboration XX (2014).

How difficult it is to make our results compatible with the *Planck* CMB constraints is illustrated in Fig. 12. There we show the predicted XLF for the *Planck* CMB cosmology compared to the one observed in the REFLEX survey. The dramatic difference in cluster number counts is apparent. It has already been discussed in the *Planck* paper on cosmological results from clusters (Planck Collaboration XX 2014) how the results could be reconciled very roughly by allowing a mass bias of 45% (that is assuming that the X-ray mass determination covers on average only 55% of the true mass of a cluster). This assumption is included in the result shown in Fig. 12. It gives a rough agreement, but the value for the mass bias is far outside the range of acceptable values. In the comparison of X-ray-determined masses with mass measurements from gravitational lensing (Mahdavi et al. 2013; Zhang et al. 2010; Okabe et al. 2010), one finds small biases with X-ray masses lower by few percent to about 20%. The large mass bias needed above is not compatible with these observational results. We also note in Fig. 11 that the cluster result has an overlap with the WMAP CMB data.

We can also compare our results with previous X-ray cluster studies by Vikhlinin et al. (2009); Henry et al. (2009); and Mantz et al. (2008). The cosmological analysis of Vikhlinin et al. (2009) is based on a nearby sample of 49 clusters selected from the brightest clusters in the sky with $\langle z \rangle \leq 0.05$ and a more distant cluster sample of 37 clusters from the 400 deg^2 survey (Burenin et al. 2007) with $\langle z \rangle \geq 0.55$. All clusters are well observed with *Chandra* so that masses can be estimated from low scatter mass proxies, such as gas mass, M_{gas}, and the product of

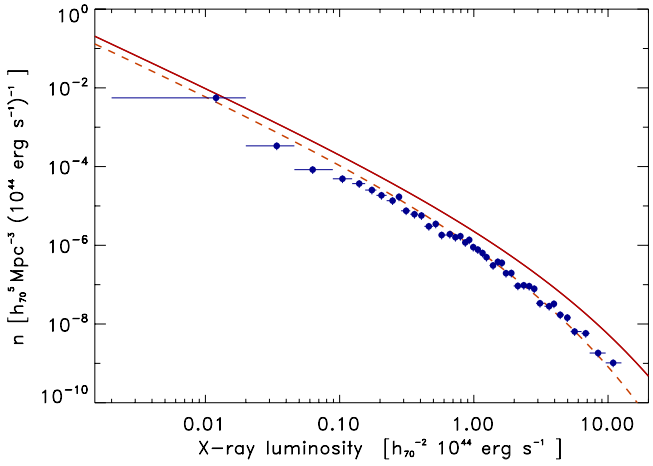

Fig. 12. Comparison of the observed REFLEX II luminosity function (data points) with the theoretical prediction for the best fitting model to the *Planck* CMB data (Planck Collaboration XVI 2014) with Ω_m = 0.315 and σ_8 = 0.834 with a mass bias of 10% (upper solid line). Same calculation but assuming a mass bias of 45% is shown by the lower dashed line.

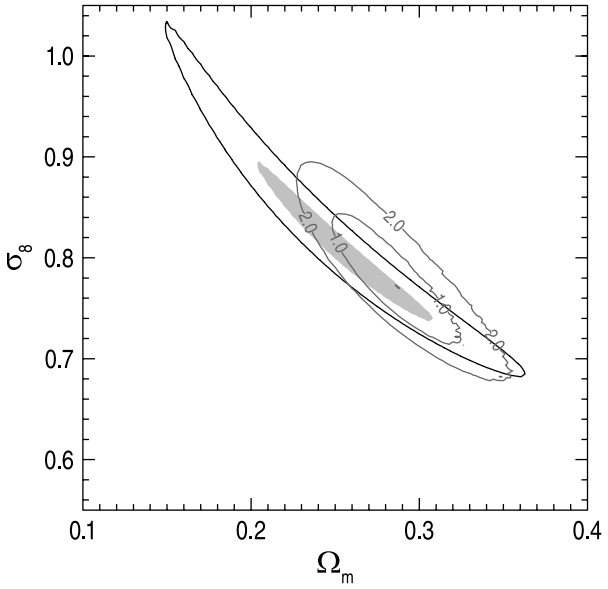

Fig. 13. Comparison to the results from the X-ray cluster survey by Vikhlinin et al. (2009). The constraints on Ω_m and σ_8 shown here have been derived from the low redshift sample of 49 clusters at $\langle z \rangle$ = 0.05 of their survey. 1 and 2σ contours are shown for both surveys.

gas mass and bulk temperature, Y_X. While the full set of data is used to obtain information on the equation of state parameter of Dark Energy, w, the parameters Ω_m and σ_8 are best constraint by the low redshift sample alone, as discussed in their paper. In Fig. 13 we compare their results to ours and find very good agreement. Our results are better constrained along the degeneracy direction, thanks to the better information we have on the shape of the XLF.

Also the work by Henry et al. (2009) uses a small sample of local clusters with a better mass proxy than X-ray luminosity, which is the spectroscopically measured intracluster medium temperature from X-ray observations. Their sample comprises 48 of the brightest clusters in the sky (from HIFLUGCS, Reiprich & Böhringer 2002) with temperatures measured with the ASCA Satellite taken from Horner et al. (2001) and Ikebe et al. (2002) with $z \leq 0.2$ and $k_B T \geq 3$ keV. The results obtained by marginalizing over 12 uninteresting

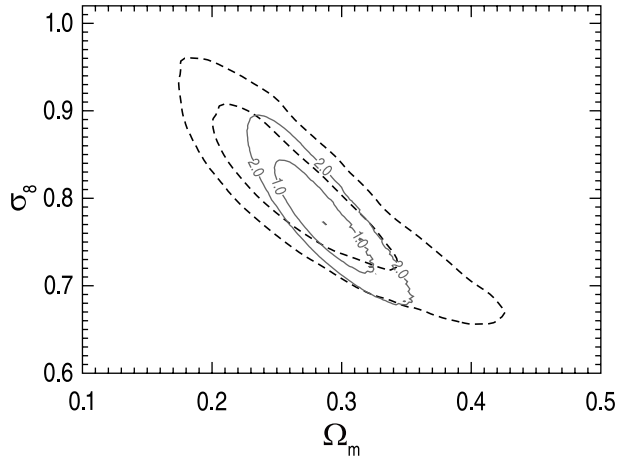

Fig. 14. Comparison to constraints from SDSS MaxBCG clusters (Rozo et al. 2010). The more than 10 000 clusters cover a redshift range of z = 0.1–0.3 and an approximate mass range of $M = 7 \times 10^{13}$–2×10^{15} $M_\odot$.

parameters are characterized by very elongated error ellipses (see their Fig. 10) for which the authors provide the parameterization, $\sigma_8 \left(\frac{\Omega_m}{0.32}\right)^{0.3} = 0.86(\pm 0.04)$. Our results shown in Fig. 10 are best characterized by $\sigma_8 \left(\frac{\Omega_m}{0.27}\right)^{0.57} = 0.80(\pm 0.03)$. Transforming both relations to the same pivot point in the middle, we find $\sigma_8 \left(\frac{\Omega_m}{0.30}\right)^{0.3} = 0.877(\pm 0.04)$ for the results of Henry et al. (2009) and $\sigma_8 \left(\frac{\Omega_m}{0.30}\right)^{0.57} = 0.753(\pm 0.03)$ for our work. This displays an offset between the two results of almost 2σ. The data used by Henry et al. (2009) stem from the pre-*Chandra*/*XMM-Newton* era without good spatially resolved spectroscopy. Thus the small difference between these results and ours is not a reason for concern.

For their analysis Mantz et al. (2008) use 130 clusters from REFLEX I with a lower luminosity cut of $L_X = 2.55 \times 10^{44}\ h_{70}^{-2}$ erg s^{-1} in the 0.1–2.4 keV band, 78 clusters from the northern BCS sample, and 34 clusters from MACS with a flux limit of $F_X = 2 \times 10^{-12}$ erg cm^{-2} s^{-1}. The cosmological constraints on the two parameters Ω_m and σ_8 from an analysis of the cluster data alone marginalizing over a comprehensive set of other parameters is shown in their Fig. 7. Our error ellipse from Fig. 10 falls nicely in the middle of their constraints region. At Ω_m = 0.27 their constraints are $\sigma_8 = 0.805 \pm 0.1$ for example in very close agreement to our results.

Rozo et al. (2010) derived constraints for cosmological parameters from an analysis of the galaxy cluster population in the Sloan Digital Sky Survey (SDSS) obtained by means of the MaxBCG cluster detection method (Koester et al. 2007). A total of 10 810 galaxy clusters are used in the redshift range z = 0.1–0.3 from a survey area of 7398 deg^2 of SDSS-DR4+. While there are many more cluster in the sample than in any other survey discussed here, the scatter in the richness – mass relation is much greater than for the X-ray related mass proxies. The richness mass relation is calibrated by an analysis of gravitational lensing data of stacked cluster shear profiles from SDSS. In Fig. 14 we compare our results to their constraints and note a very good overlap.

In Fig. 15 we then compare our results to the set of the X-ray and optical results discussed above, where the constraints from the literature have been tightened further by combining the cluster constraints with those of WMAP 5 yr data (Dunkley et al. 2009). For the display of our results we use our preferred $L_X - M$ scaling relation from Fig. 8 neglecting the uncertainties of

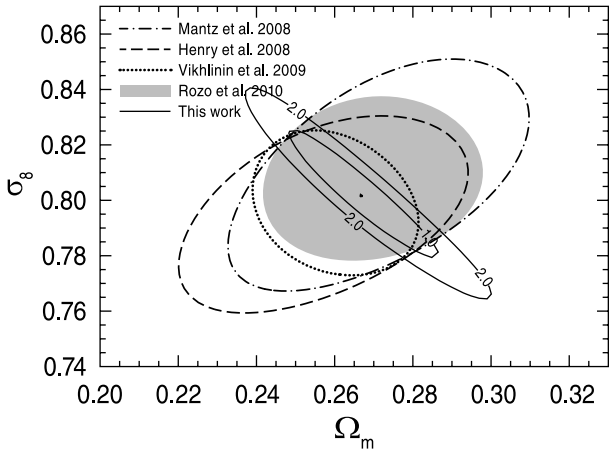

Fig. 15. Comparison to optical and X-ray surveys, where the data have been combined with WMAP 5 yr data (Rozo et al. 2010; Mantz et al. 2008; Vikhlinin et al. 2009; Henry et al. 2009). Our data are the REFLEX constraints with no marginalization over scaling relation systematics. The contours for the literature data give 68% confidence limits and for the REFLEX II data 1 and 2σ contours are shown.

this relation. We note that this relation shows prefect consistency with the other cosmological data. Thus when using additional constraints from the CMB anisotropies we are pointed towards an observable – mass relation for our clusters which agrees very well with the default relation used in this paper.

In our work, the good characterization of the shape of the XLF is the way to break the degeneracy between the σ_8 and Ω_m parameters. Another way to get a better separation between the two parameters is to extend the cluster study to higher redshifts. This has recently been achieved in ground-based microwave surveys, detecting clusters in the SZE. Thus to compare our findings to their results provides another independent consistency check of our approach. From the cluster sample detected with the South Pole Telescope (SPT), Benson et al. (2013) obtained cosmological parameter constraints from 18 massive clusters in the redshift range $z = 0.3$ to 1.1. Our constraints fall very nicely into the middle of their constraints using an H_0 prior and Big Bang nucleosynthesis results. Our results also overlap well with the combined constraints of SPT cluster and WMAP CMB data. The other distant SZE cluster sample comes from the microwave background survey with the Atacama Cosmology Telescope (ACT). Cosmological constraints have recently been derived by Hasselfeld et al. (2013) from 15 massive clusters in the redshift range $z = 0.2$–1.4. Our results overlap with their constraints in the lower half of their contours at lower σ_8.

9. Summary and conclusions

We used the REFLEX II catalogue and the well defined selection function to construct the X-ray luminosity function for the sample at a median redshift of $z = 0.102$. For the flux limit of $F_X = 1.8 \times 10^{-12}$ erg s^{-1} cm^{-2}, a luminosity limit of $L_X = 0.03 \times 10^{44}$ erg s^{-1} (for 0.1–2.5 keV), a lower photon count limit of 20 source photons, and a redshift range of $z = 0$–0.4, some 819 clusters are included in the luminosity function determination. The cluster catalogue is better than 90% complete, with a best estimate of about 95% as detailed in Böhringer et al. (2013) and we also expect a few percentage points of contamination by clusters whose X-ray luminosity may be boosted by an AGN. Since this fraction is small, and since an incompleteness even of the order of 10% causes only little change in the derived cosmological parameters as explained in Sect. 7, we have not included any correction for incompleteness in the results we have presented.

Inspecting the XLF in different redshift shells reveals no significant evolution of the XLF. We showed for our best fitting cosmological model that this undetectable change is consistent with the theoretical expectation. This does not imply that there is no evolution in the cluster mass function. There are two competing effects, the evolution of the mass function and the evolution of the $L_X - M$ relation. The relation of X-ray luminosity to mass evolves because clusters have been more compact on average in the past, which increases the X-ray luminosity (through the square-law dependence on the density), and clusters of the same mass become brighter. This compensates for the loss of massive clusters at higher redshifts and suppresses the evolution in X-ray luminosity.

In search of a good analytical description of the XLF, we found that the Schechter function does not capture our knowledge with sufficient precision. We therefore proposed a modified Schechter function for a good description of the data.

The most interesting application of the XLF is to test theoretical predictions of this function within the framework of different cosmological models. These tests are based on the theory of cosmic evolution and structure formation and rely, among other things, on the description of the transfer function of the power spectrum by Eisenstein & Hu (1998), on the numerical simulation calibrated recipe for the cluster mass function by Tinker et al. (2008), and on scaling relations that enable the connection of cluster mass and X-ray luminosity. Unlike the scaling relations, the other theoretical framework has been intensively tested and is believed to be accurate at about the 5% level.

We found that we can get a very good match of the observed XLF to the theoretical predictions for a very reasonable cosmological model; in particular if we restrict the fitting to the luminosity range $L_X \geq 0.25 \times 10^{44}$ erg s^{-1} (0.1–2.4 keV) where we have an observationally calibrated $L_X - M$ relation (note the good match of the predicted and observed XLF in Fig. 7). In using the observational data to constrain cosmological parameters, we have in this paper not pursued a comprehensive marginalization over all relevant parameters. We postpone this to a later work. We instead wanted to gain an overview and an understanding of the effect of the different parameters by studying them individually. From this investigation it becomes clear that by far the largest uncertainty in the constraints of cosmological parameters is introduced by the $L_X - M$ scaling relation, specifically by its slope and normalization. We gave a detailed account of the influence of the other parameters and then concentrated on a marginalization study that includes these two most important input parameters, which provides a good account of the overall uncertainties. The important constraints that we derived from the REFLEX II data are $\Omega_m = 0.29 \pm 0.04$ for the matter density parameter and $\sigma_8 = 0.77 \pm 0.07$ for the amplitude parameter of the matter density fluctuations.

The currently most interesting comparison of our findings with other results is with the recently published cosmological constraints from clusters detected with *Planck* (Planck Collaboration XVI 2014). The *Planck* results show a tension between the cosmological constraints on Ω_m and σ_8 from clusters and from the CMB anisotropies, which has caused a lively debate. We find that our results agree perfectly with the *Planck* cluster data and it would be very hard to reconcile them with the CMB derived results. However, we find that our results are consistent with the constraints from the CMB study with WMAP (Hinshaw et al. 2013). Since there is also some tension between

the implications from the CMB data of WMAP and *Planck*, the source of which is currently under investigation, we are confident, that the solution of these problems will bring closer agreement of all the data in the future without a significant change in our results.

The good agreement of our results with the recent work on cluster cosmology in the literature is encouraging. But we should point out here that our new results provide tighter constraints on the two tested parameters than the previous studies and constitute a significant improvement. We have, however, reached a limit where a further increase in the clusters sample and in the overall statistics will not lead to many more improvements, if we cannot calibrate the scaling relations better. A major reason for our poor knowledge of the scaling relations originates in several facts. On one hand the cluster samples with very well defined selection criteria used in the scaling relation studies are still very small with typically 30 to 50 objects. Another source of uncertainty is revealed by the difference in results for mass, temperature, or X-ray luminosity determined for the same set of clusters by different authors (e.g. Reichert et al. 2011). And there are still some calibration uncertainties for the *XMM-Newton* and *Chandra* instruments for which there is an ongoing effort of their resolution (e.g. Kettula et al. 2013). Therefore one of the next major efforts of the authors will be to increase the sample size and the data reduction quality of the cluster samples to obtain better constraints on the important scaling relations.

Acknowledgements. We would like to thank the ROSAT team at MPE for the support with the data and with advice in the reduction of the RASS, and to thank the staff at ESO La Silla for the technical support during the numerous observing runs conducted for the REFLEX project since 1992. Special thanks goes to Peter Schuecker, who was a very essential part of our team and who died unexpectedly in 2006. H.B. and G.C. acknowledge support from the DFG Transregio Program TR33 and the Munich Excellence Cluster "Structure and Evolution of the Universe". C.A.C. acknowledges STFC for financial support.

Appendix A: Expected evolution of the X-ray luminosity function

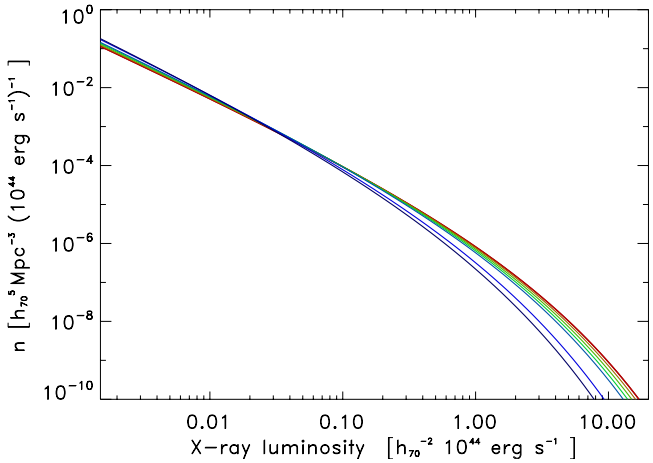

Fig. A.1. Predicted evolution of the X-ray luminosity function of galaxy clusters. The curves from top to bottom show the XLF for z = 0, 0.1, 0.2, 0.3, 0.4 0.8, 1.0.

Since we could not detect a significant evolutionary effect of the luminosity function as a function of redshift in the REFLEX II sample in our analysis in this paper, we take a closer look at the expected evolution. The evolution is driven by building up the mass of clusters increasing the high mass end of the cluster mass function with time. But this evolutionary effect is partly conteracted by the evolution of the $L_X - M$ relation, so that the XLF shows very little evolution at low redshifts. This is illustrated in Fig. A.1 which shows the predicted XLF at redshifts from z = 0 to 0.4 and at z = 0.8 and 1. We note that only if we can probe the high mass end of the XLF very precisely at low redshift, we can probe for this weak effect. Owing to the small volume of the survey at low redshifts, we do not have the statistics to probe the high mass end sufficiently, and thus we have no good leverage to constrain the luminosity function evolution. This does not imply, however, that there is no evolution of the cluster mass function.

Appendix B: Shape dependence of the XLF on various parameters

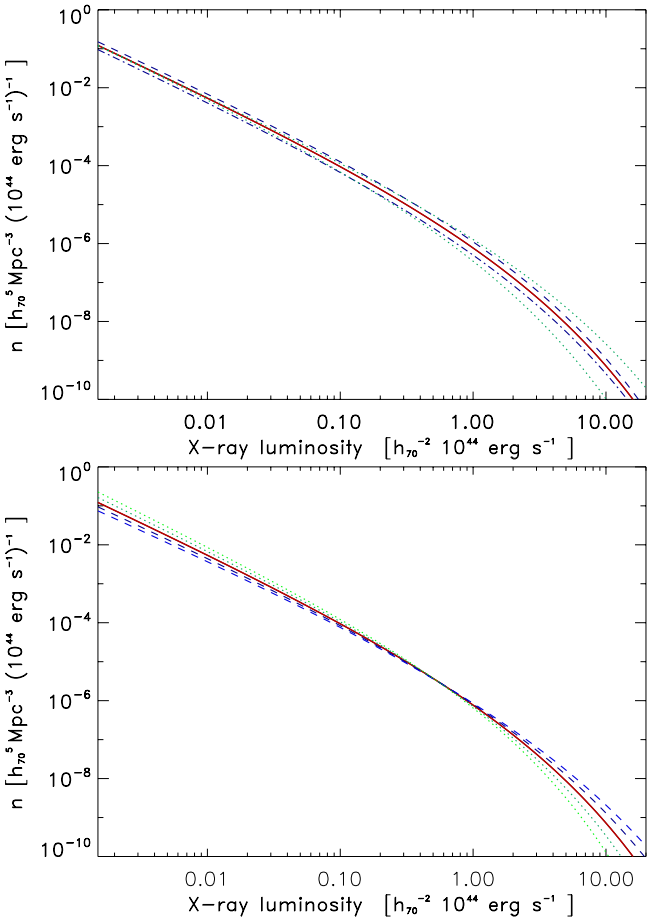

Fig. B.1. *Upper panel*: variations of the predicted XLF with the change in the parameters Ω_m and σ_8. The reference model (solid red line) has Ω_m = 0.26 and σ_8 = 0.8, the dashed line has Ω_m = 0.30 and the dot-dashed line Ω_m = 0.22, while the upper dotted line shows the result for σ_8 = 0.9 and the lower one for σ_8 = 0.7. *Lower panel*: Variations of the predicted XLF with the change in the parameter, α_{sl} of the $L_X - M$ scaling relation. The reference model (solid red line) has α_{sl} = 1.51, the two dashed lines correspond to α_{sl} = 1.61 and 1.71 and the two dotted lines to α_{sl} = 1.41 and 1.31.

In this section we show how the XLF depends on the cosmological parameters Ω_m and σ_8, on the one hand, and on the slope and normalization parameter of the $L_X - M$ scaling relation, on the other, to explain the behaviour of the parameter constraints in Sect. 5. Figure B.1 gives the effect of the cosmological

parameters in the upper panel and in the lower panel the effect of the scaling relation parameters. We can see that e.g. an increase in the slope of the scaling relation makes the XLF steeper. This can be compensated for by a larger σ_8 and a smaller Ω_m to keep the fit to the observed XLF in balance.

References

Allen, S. W., Schmidt, R. W., Fabian, A. C., et al. 2003, MNRAS, 342, 287
Allen, S. W., Evrard, A. E., & Mantz, A. B. 2011, ARA&A, 49, 409
Arnaud, M., Pratt, G. W., Piffaretti, R., et al. 2010, A&A, 517, 92
Balaguera-Antolinez, A., Sanchez, A., Böhringer, H., et al. 2011, MNRAS, 413, 386
Balaguera-Antolinez, A., Sanchez, A., Böhringer, H., et al. 2012, MNRAS, 425, 2244
Benson, B. A., de Haan, T., Dudley, J. P., et al. 2013, ApJ, 763, 147
Böhringer, H. 2011, AIP Conf. Proc., 1381, 137
Böhringer, H., Voges, W., Huchra, J. P., et al. 2000, ApJS, 129, 435
Böhringer, H., Schuecker, P., Guzzo, L., et al. 2001, A&A, 369, 826
Böhringer, H., Collins, C. A., Guzzo, L., et al. 2002, ApJ, 566, 93
Böhringer, H., Schuecker, P., Guzzo, L., et al. 2004, A&A, 425, 367
Böhringer, H., Schuecker, P., Pratt, G. W., et al. 2007, A&A, 469, 363
Böhringer, H., Pratt, G. W., Arnaud, M., et al. 2010, A&A, 514, A32
Böhringer, H., Dolag, K., & Chon, G., 2012, A&A, 539, A120
Böhringer, H., Chon, G., Collins, C. A., et al. 2013, A&A, 555, A30
Borgani, S., Rosati, P., Tozzi, P., et al. 2001, ApJ, 561, 13
Burenin, R. A., Vikhlinin, A., Hornstrup, A., et al. 2007, ApJS, 172, 561
Burke, D. J., Collins, C. A., Sharples, R. M., et al. 1997, ApJ, 488, L83
Burns, J. O., Ledlow, M. J., Loken, C., et al. 1996, ApJ, 467, L49
Chon, G., & Böhringer, H. 2012, A&A, 538, A35
Chon, G., & Böhringer, H. 2013, MNRAS, 429, 3272
Collins, C. A., Burke, D. J., Romer, A. K., et al. 1997, ApJ, 479, L117
Collins, C. A., Guzzo, L., Böhringer, H., et al. 2000, MNRAS, 319, 939
Croston, J. H., Pratt, G. W., Böhringer, H., et al. 2008, A&A, 487, 431
Daley, D. J., & Vere-Jones, D., 1988, An Introduction to the Theory of Point Processes (New York: Springer)
de Grandi, S., Böhringer, H., Guzzo, L., et al. 1999, ApJ, 514, 148
Dickey, J. M., & Lockman, F. J., 1990, ARA&A, 28, 215
Donahue, M., Mack, J., Scharf, C., et al. 2001, ApJ, 552, L93
Dunkley, J., Spergel, D. N., Komatsu, E., et al. 2009, ApJS, 180, 306
Ebeling, H., Edge, A. C., Fabian, A. C., et al. 1997, ApJ, 479, 101
Edge, A. C., Stewart, G. C., Fabian, A. C., et al. 1990, MNRAS, 245, 559
Eisenstein, D. J., & Hu, W., 1998, ApJ, 496, 605
Gioia, I. M., Maccacaro, T., Schild, R. E., et al. 1984, ApJ, 283, 495
Gioia, I. M., Henry, J. P., Mullis, C. R., et al. 2001, ApJ, 553, L105
Guzzo, L., Schuecker, P., Böhringer, H.,et al. 2009, A&A, 499, 357
Hasselfield, M., Hilton, M., Marriage, T. A., et al. 2013, J. Cosmol. Astro-Part. Phys., 7, 8
Henry, J. P., 2004, ApJ, 609, 603
Henry, J. P., Gioia, I. M., Maccacaro, T., et al. 1992, ApJ, 386, 408
Henry, J. P., Evrard, A. E., Hoekstra, H., et al. 2009, ApJ, 691, 1307
Hinshaw, G., Larson, D., Komatsu, E., et al. 2013, ApJS, 208, 19
Horner, D. J. 2001, Ph.D. Thesis, Univ. Maryland
Hu, W., & Kravtsov, A. V., 2003, ApJ, 584, 702
Ikebe, Y., Reiprich, T. H., Böhringer, et al. 2002, A&A, 383, 773
Kerscher, M., Mecke, K., Schuecker, P., et al. 2001, A&A, 377, 1
Kettula, K., Nevalainen, J., & Miller, E. D. 2013, A&A, 552, A47
Koens, L. A., Maughan, B. J., Jones, L. R., et al. 2013, MNRAS, 435, 3231
Koester, B. P., McKay, T. A., Annis, J., et al. 2007a, ApJ, 660, 239
Komatsu, E., Smith, K. M., Dunkley, J., et al. 2011, ApJS, 192, 18
Kowalski, M. P., Ulmer, M. P., Cruddace, R. G., et al. 1984, ApJS, 56, 403
Ledlow, M. J., Loken, C., & Burns, J. O., 1999, ApJ, 516, L53
Mahdavi, A., Hoekstra, H., Babul, A., et al. 2013, ApJ, 767, 116
Mantz, A., Allen, S. W., Ebeling, H., et al. 2008, MNRAS, 387, 1179
Marriage, T. B., Acquaviva, V., Ade, P. A. R., et al. 2011, ApJ, 737 61
Maughan, B., 2007, ApJ, 668, 772
Marshall, H. L., Avni, Y., Tannanbaum, H., & Zamorani, G. 1983, ApJ, 269, 35
Melin, J.-B., Bartlett, J. G., Delabrouille, J., et al. 2011, A&A, 525, A139
Meneghetti, M., Rasia, E., Merten, J., et al. 2010, A&A, 514, A93
Mullis, C. R., Vikhlinin, A., Henry, J. P., et al. 2004, ApJ, 607, 175
Nagai, D., Vikhlinin, A., & Kravtsov, A. V., 2007, ApJ, 655, 98
Navarro, J., Frenk, C. S., & White, S. D.M. 1995, MNRAS, 275, 56
Navarro, J., Frenk, C. S., & White, S. D.M., 1997, ApJ, 490, 493
Nichol, R. C., Romer, A. K., Holden, B. P., et al. 1999, ApJ, 521, L21
Okabe, N., Zhang, Y.-Y., Finoguenov, A., et al. 2010, ApJ, 721, 875
Ortiz-Gil, A., Guzzo, L., Schuecker, P., et al. 2004, MNRAS, 348, 325
Planck Collaboration VIII. 2011, A&A, 536, A8
Planck Collaboration XX. 2014, A&A, in press, DOI: 10.1051/0004-6361/201321521
Planck Collaboration XVI. 2014, A&A, in press, DOI: 10.1051/0004-6361/201321591
Pratt, G. W., Croston, J. H., Arnaud, M., et al. 2009, A&A, 498, 361
Pratt, G. W., Arnaud, M., Piffaretti, R., et al. 2010, A&A, 511, A85
Piccinotti, G., Mushotzky, R. F., Boldt, E. A., et al. 1982, ApJ, 253, 485
Reichardt, C. L., Stadler, B., Bleem, C. E., et al. 2013, ApJ, 763, 127
Reichert, A., Bhringer, H., Fassbender, R., Mhlegger, M., 2011, A&A, 535, A4
Reiprich T. H., & Böhringer, H., 2002, ApJ, 567, 716
Rosati, P., Della Ceca, R., Norman, C., et al. 1998, ApJ, 492, L21
Rosati, P., Borgani, S., Norman, C., 2002, ARA&A, 40, 539
Rozo, E., Wechsler, R. A., Rykoff, E. S., et al. 2010, ApJ, 708, 645
Sarazin, C. L. 1986, Rev. Mod. Phys., 58, 1
Schuecker, P., & Böhringer, H., 1998, A&A, 339, 315
Schuecker, P., Böhringer, H., Guzzo, L., et al. 2001, A&A, 368, 86
Schuecker, P., Guzzo, L., Collins, C. A., et al. 2002, MNRAS, 335, 807
Schuecker, P., Böhringer, H., Collins, C. A. et al. 2003a, A&A, 398, 867
Schuecker, P., Caldwell, R. R., Böhringer, H., et al. 2003b, A&A, 402, 53
Sehgal, N., Trac, H., Acquaviva, V., et al. 2011, ApJ, 732, 44
Spergel, D. N., Verde, L., Peiris, H. V., et al. 2003, ApJS, 148, 175
Tinker, J., Kravtsov, A. V., Klypin, A., et al. 2008, ApJ, 688, 709
Tinker, J. L., Robertson, B. E., Kravtsov, A. V., et al. 2010, ApJ, 724, 878
Valdarnini, R., & Piffaretti, R., 2010, AIP Conf., 1248, 304
Vikhlinin, A., McNamara, B. R., Forman, W., et al. 1998, 498, L21
Vikhlinin, A., Kravtsov, A. V., Burenin, R. A., et al. 2009, ApJ, 692, 1060
Voevodkin, A., & Vikhlinin, A., 2004, ApJ, 601, 610
Voit, M. 2005, Rev. Mod. Phys., 77, 207
Voges, W., Aschenbach, B., Boller, T., et al. 1999, A&A, 349, 389
Trümper, J. 1993, Science, 260, 1769
Zhang, Y.-Y., Okabe, N., Finoguenov, A., et al. 2010, ApJ, 711, 1033